NONLINEAR VIBRATION ANALYSIS OF THE SMALLSAT SPACECRAFT: FROM IDENTIFICATION TO DESIGN

T. Detroux, J.P. Noël, L. Masset, G. Kerschen

Space Structures and Systems Laboratory
Aerospace and Mechanical Engineering Department
University of Liège

Allée de la découverte 9, 4000, Liège, Belgium
E-mail: tdetroux, jp.noel, luc.masset, g.kerschen@ulg.ac.be

ABSTRACT

The objective of the present contribution is to introduce nonlinear experimental and numerical tools and methods applicable to real-life structures. The study is illustrated using the SmallSat spacecraft developed by Airbus Defence and Space, which possesses several localized nonlinearities. The computation of nonlinear normal modes and bifurcations reveals that the satellite possesses complex dynamics including modal interactions, quasiperiodic oscillations and isolated resonances.

1. INTRODUCTION

Recent years have witnessed a great increase in the number of spacecraft measurement campaigns where engineers were confronted with the existence of nonlinear behavior. However, current practice in industry is still to ignore nonlinearities, arguably because their analysis is regarded as impractical. To thoroughly investigate the intrinsic features of real-world structures vibrating in nonlinear regimes of motion, the nonlinear analysis framework presented in Fig. 1 is adopted in this paper. It builds on several successive steps:

1. **Measure**

The measurement campaign usually serves two purposes. First, experimental data are used to reveal nonlinear behaviors or to confirm their presence. The second objective is to acquire experimental data sets for the identification step. Because the response of a nonlinear system does not scale with the amplitude of the input, data should be measured at several excitation levels. While data obtained at low level may help study the underlying linear model, data at high level usually capture nonlinearities more accurately.

2. **Identify a nonlinear model**

During this step, a nonlinear model of the structure that possesses good predictive capability is sought. The nonlinearities are first identified from the experimental data using techniques such as the restoring force surface (RFS) method [1], the reverse path method [2] or nonlinear subspace identification [3]. The nonlinearities are then introduced in an updated finite element model that describes the underlying linear structure.

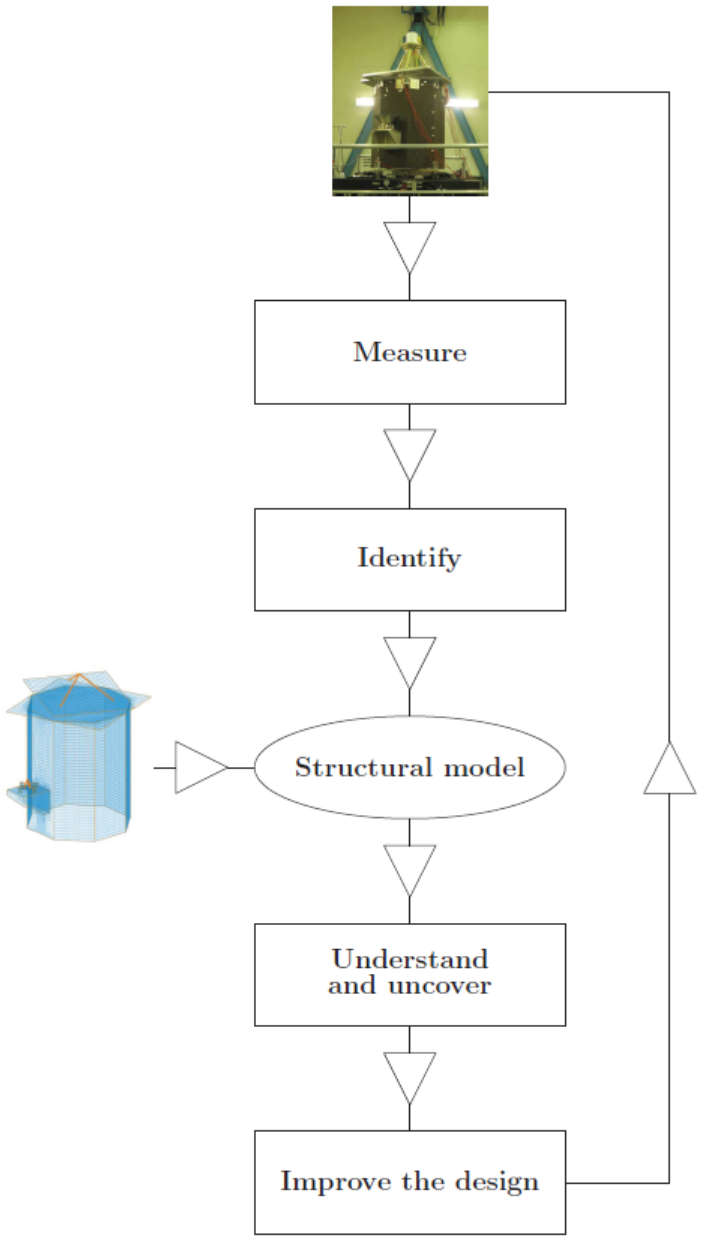

Fig. 1. Design cycle of nonlinear engineering structures, from measurements to design.

3. Understand and uncover nonlinear phenomena

The identified model is exploited for understanding the dynamics observed experimentally but also for uncovering nonlinear phenomena that could have been missed during the test campaign. Direct time integration methods can be used, such as Runge-Kutta or Newmark schemes [4], but we propose to exploit the bifurcation and modal analysis methodology developed in [5] for an easier and more thorough interpretation.

4. Improve the structural design

From the observations made during the previous step, the structural analyst can precisely quantify the impact of nonlinearities. If design modifications are necessary to achieve the requested system performance, we propose to utilize bifurcation tracking for the update of selected design parameters.

The outlined design methodology is demonstrated in this paper using a spacecraft structure, whose description is provided in Section 2. In Section 3, experimental data are analyzed to assess the nonlinear behavior of the structure. The identification of a numerical model is then described in Section 4. Based on this model and on continuation tools, Sections 5 and 6 study the nonlinear normal modes and the bifurcation curves of the system, respectively. In Section 7, bifurcation tracking is employed to improve the design of the spacecraft. Finally, the conclusions of the paper are drawn in Section 8.

2. DESCRIPTION OF THE SMALLSAT SPACECRAFT

The SmallSat structure was conceived by EADS-Astrium (now Airbus Defence and Space) as a low-cost platform for small satellites in low earth orbits [6]. It is a monocoque tube structure which is 1.2 *m* in height and 1 *m* in width. It is composed of eight flat faces for equipment mounting purposes, creating an octagon shape. The spacecraft structure supports a dummy telescope mounted on a baseplate through a tripod. A prototype of the spacecraft is represented in Fig. 2(a).

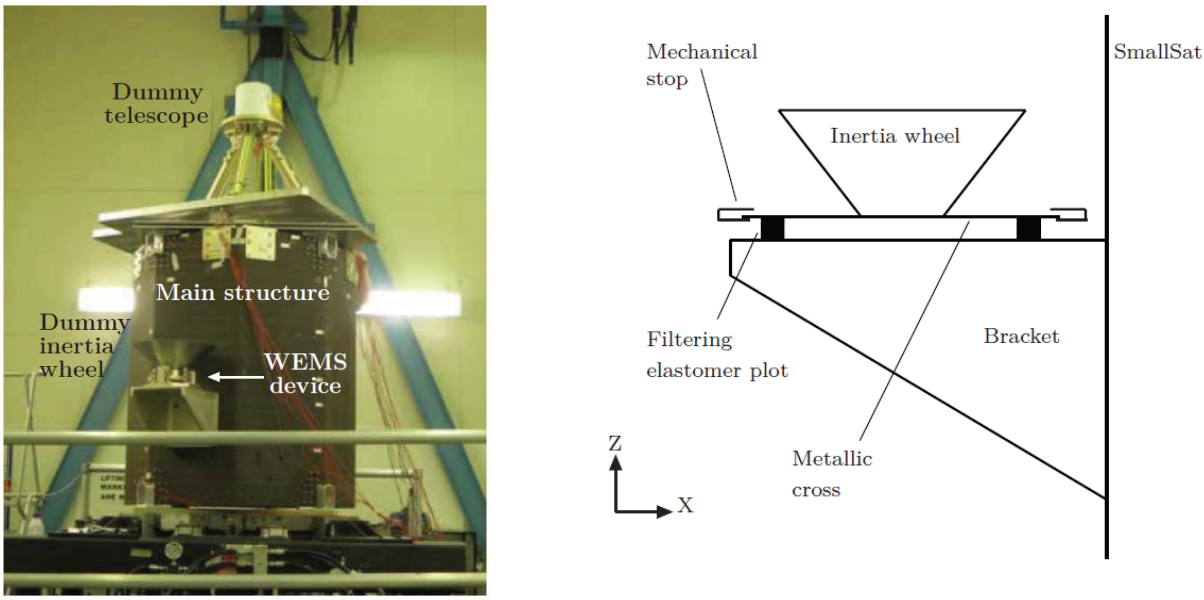

(a) (b)

Fig. 2. SmallSat spacecraft. (a) Photograph; (b) schematic of the WEMS, the nonlinear vibration isolation device.

As depicted in Fig. 2(b), a support bracket connects to one of the eight walls the so-called wheel elastomer mounting system (WEMS) which is loaded with an 8-*kg* dummy inertia wheel. The WEMS acts as a mechanical filter which mitigates high-frequency disturbances coming from the inertia wheel through the presence of a soft elastomeric interface between its mobile part, i.e., the inertia wheel and a supporting metallic cross, and its fixed part, i.e., the bracket and by extension the spacecraft. Moreover, the WEMS incorporates eight mechanical stops, covered with a thin layer of elastomer to prevent metal-metal impacts, and designed to limit the axial and lateral motions of the inertia wheel during launch. The mechanical stops account for 4 localized nonlinear connections (NC), with axial and lateral components for each NC, and give rise to the strongly nonlinear dynamical phenomena that will be studied in this paper.

3. VIBRATION TEST CAMPAIGN

The experimental data sets analyzed in this section were acquired during a test campaign carried out by Airbus Defence and Space, Siemens-LMS and the University of Liège in Stevenage, UK. It consisted of a series of swept-sine base excitations applied to the structure for different sweep rates and directions. Fig. 3 displays the raw acceleration time histories measured vertically on the instrument panel at 0.1 g and 1 g levels. For confidentiality reasons, clearances and displacements are given through dimensionless quantities throughout the paper.

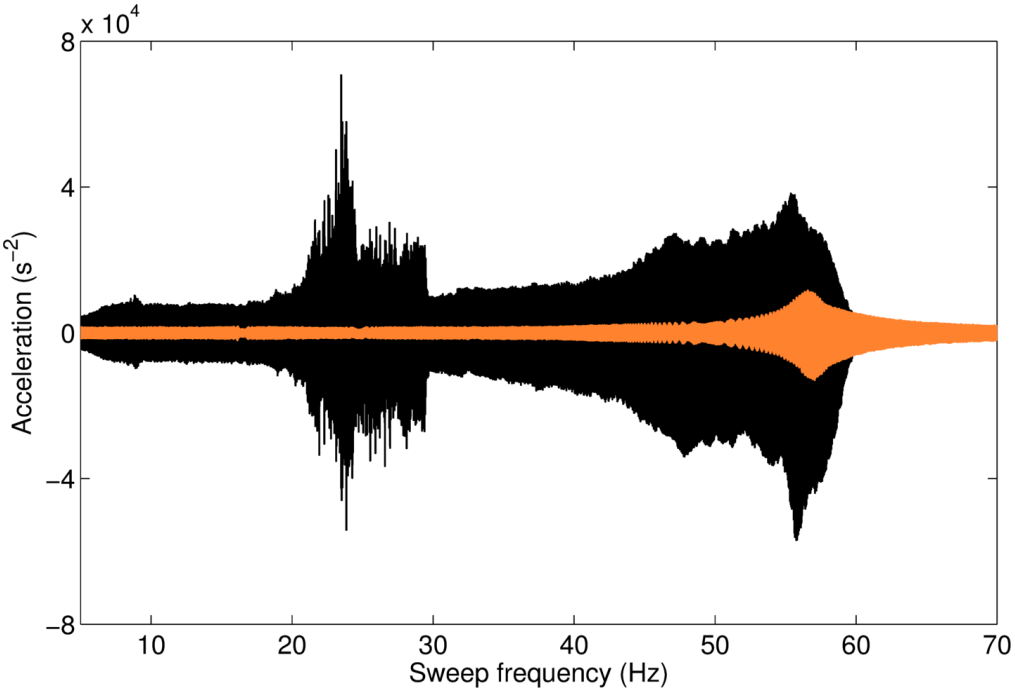

Fig. 3. Raw acceleration time histories measured on the instrumental panel at 0.1 g (in orange) and 1 g (in black) base excitation levels, obtained for a frequency sweep up.

At 0.1 g, the response at the instrument panel presents a single resonance, located around 56 Hz, which is assumed linear in view of the low level of the excitation. At 1 g, this resonance is slightly shifted to lower frequencies, but a second resonance appears between 20 and 30 Hz. A particular feature of this second resonance is that it cannot be predicted by linear modal analysis, as there exists no mode in this frequency range that involves a motion of the instrument panel [7]. Clearly, this nonlinear resonance of the instrument panel deserves further investigation, not only because it is intriguing but also because it is associated with the greatest response amplitude, at an important location due to the presence of the telescope.

4. IDENTIFICATION OF A NONLINEAR MODEL

The identification of the SmallSat's NCs of the WEMS was performed by applying the RFS method to the experimental data. Each NC was modeled using piecewise-linear functions, i.e., a trilinear spring in the axial direction (elastomer in traction/compression plus two stops), a bilinear spring in the radial direction (elastomer in shear plus one stop) and a linear spring in the third direction (elastomer in shear). For illustration, the stiffness curve identified for NC1 is displayed in Fig. 4. A clear hardening in this connection can be observed, due to the impacts of the metallic cross with the mechanical stops, together with some asymmetry, which is explained by the prestress in the elastomers due to gravity.

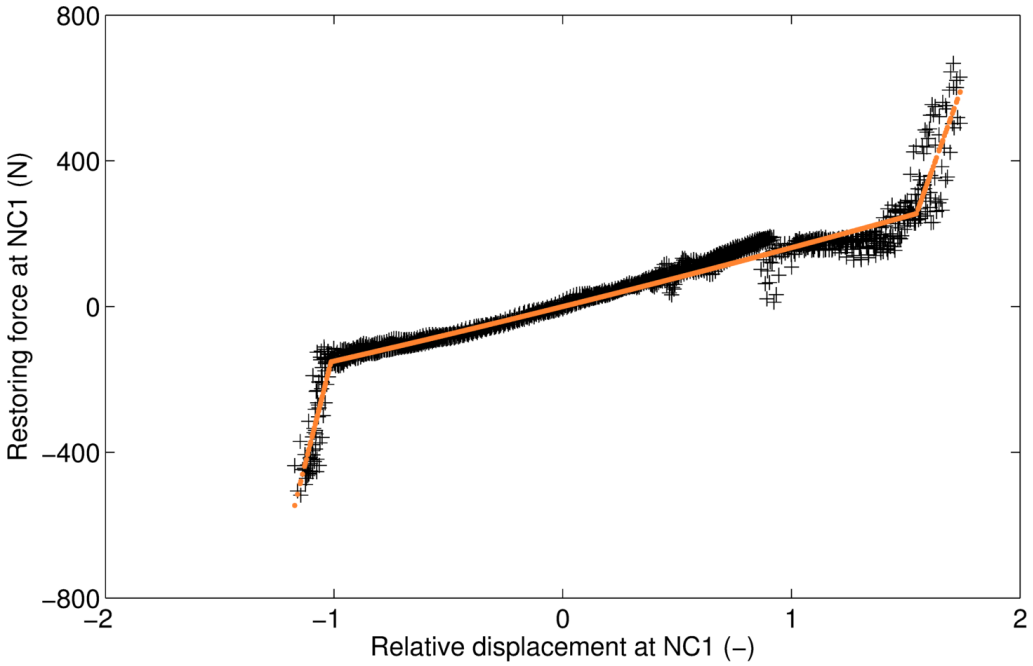

Fig. 4. Stiffness curve of NC1 identified with the RFS method (in black) and fitted with a trilinear model (in orange).

To build a complete structural model of the satellite, the identified nonlinearities, i.e., the trilinear springs in the axial direction and the bilinear springs in the lateral direction, were integrated in a detailed finite element model (FEM) of the underlying linear structure comprising 150,000 degrees of freedom (DOFs). To avoid numerical issues, C^1 continuity in the close vicinity of the clearances was enforced by regularizing the piecewise-linear functions with third-order Hermite polynomials polynomials.

The FEM, shown in Fig. 5, consists of shell elements for the main structure, the metallic cross of the WEMS device and the instrument baseplate, and point masses for the inertia wheel and the dummy telescope. Proportional damping was considered for the main structure, and the high dissipation in the elastomer plots was described using lumped dashpots of coefficients c_{ax} and c_{lat} for the axial and lateral directions, respectively. As shown in Table 1, the modes of the underlying linear structure are densely packed, and the corresponding damping ratios are all beyond 2%.

To achieve tractable calculations, the linear FEM was condensed using the Craig-Bampton reduction technique [8]. More specifically, the FEM was reduced to 10 internal modes and 9 nodes, namely both sides of each nonlinear connection and the inertia wheel, but excluding DOFs in rotation. In total, the reduced-order model hence contains 37 DOFs. The predictions of the resulting nonlinear FEM were verified to be in acceptable agreement with experimental observations for the purpose of our study [9].

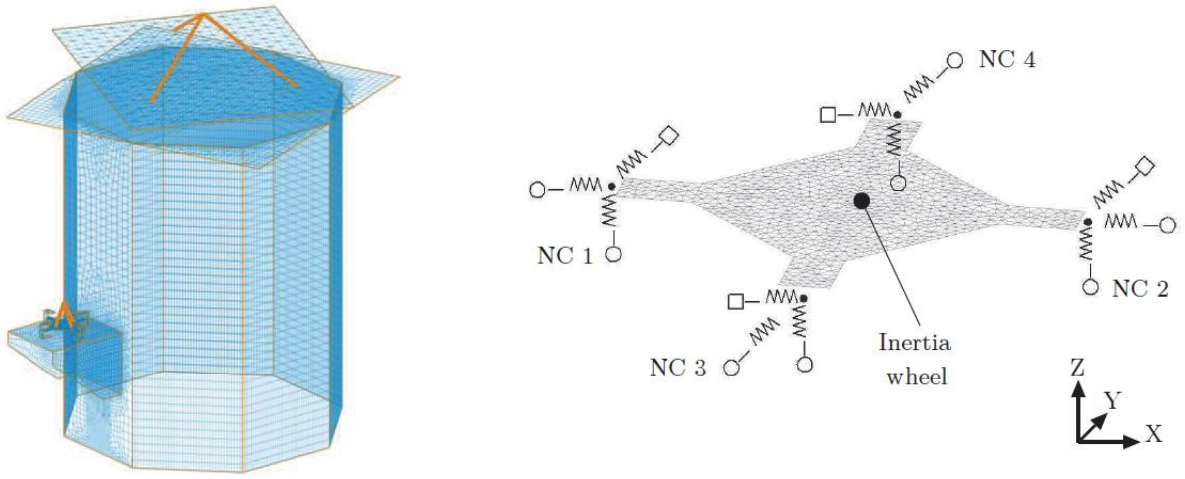

(a) (b)

Fig. 5. FEM of the SmallSat. (a) Modeling of the main structure using shell elements; (b) modeling of the WEMS using shell elements, a point mass, linear and nonlinear springs. The linear and nonlinear springs are represented with squares and circles, respectively.

Mode	Natural frequency (Hz)	Damping ratio (%)
1	8.06	10.10
2	9.14	8.03
3	20.44	11.96
4	21.60	21.04
5	22.06	11.55
6	28.75	6.23
7	32.49	2.09
8	34.78	2.23
9	39.07	2.33
10	40.78	2.42
11	45.78	2.61
12	57.76	3.13

Table 1. Linear resonance frequencies and damping ratios computed from the numerical model.

To reproduce, at least qualitatively, the experimental time series, a swept-sine excitation (0.5 Hz/min) was applied vertically to the inertia wheel, and Newmark's method used the developed model to calculate the structural response to this excitation. A sampling rate of 3000 Hz was selected for an accurate representation of the higher harmonics of the fundamental forcing frequency. The vertical acceleration of the central node on the instrument panel (P-Z) is shown in Fig. 6(a) for two forcing levels. It is clearly seen that the large-amplitude resonance at 29 Hz observed for 80 N is nonexistent at 20 N. This behavior is fully consistent with the observations made in Fig. 3.

Fig. 6(b) depicts the vertical displacement of the node located at NC1 on the inertia wheel side (NC1-Z) for forcing amplitudes of 168 N, 170 N, 172 N and 174 N. If the classical jump in amplitude in the vicinity of the resonance can be observed in this figure, a sudden shift of the resonance frequency is also noticed when the forcing amplitude increases from 170 N to 172 N.

This nonlinear phenomenon, which is not often discussed in the literature, deserves deeper investigations, as it is associated with a substantial variation of the resonance frequency. Finally, we note in all time series of Fig. 6(b) the presence of an unexpected modulation of the responses envelope between 30 and 31 Hz.

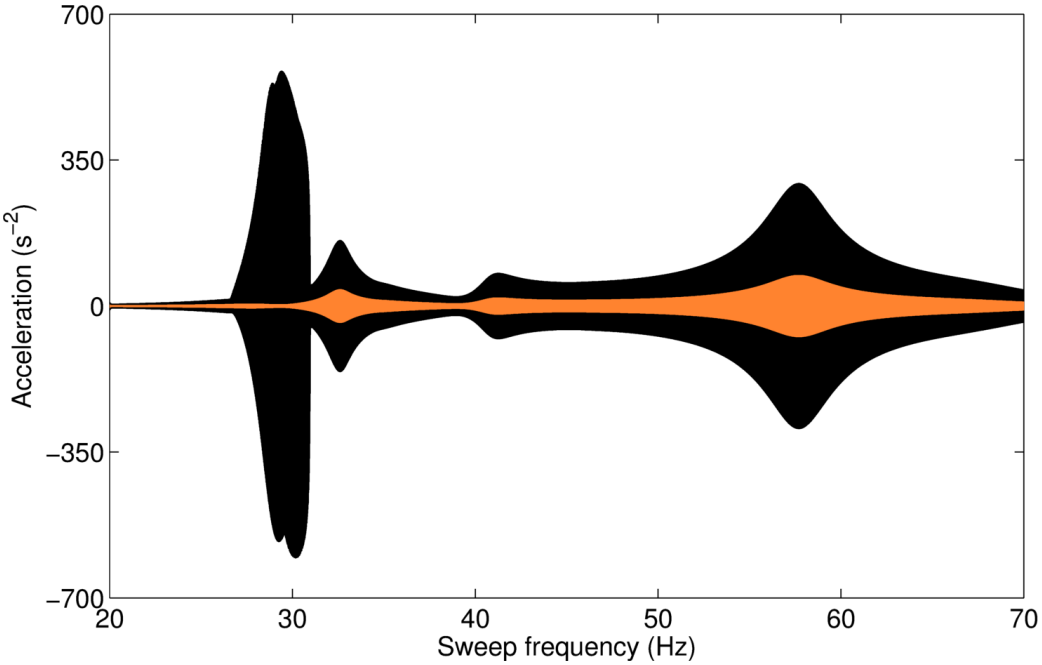

(a)

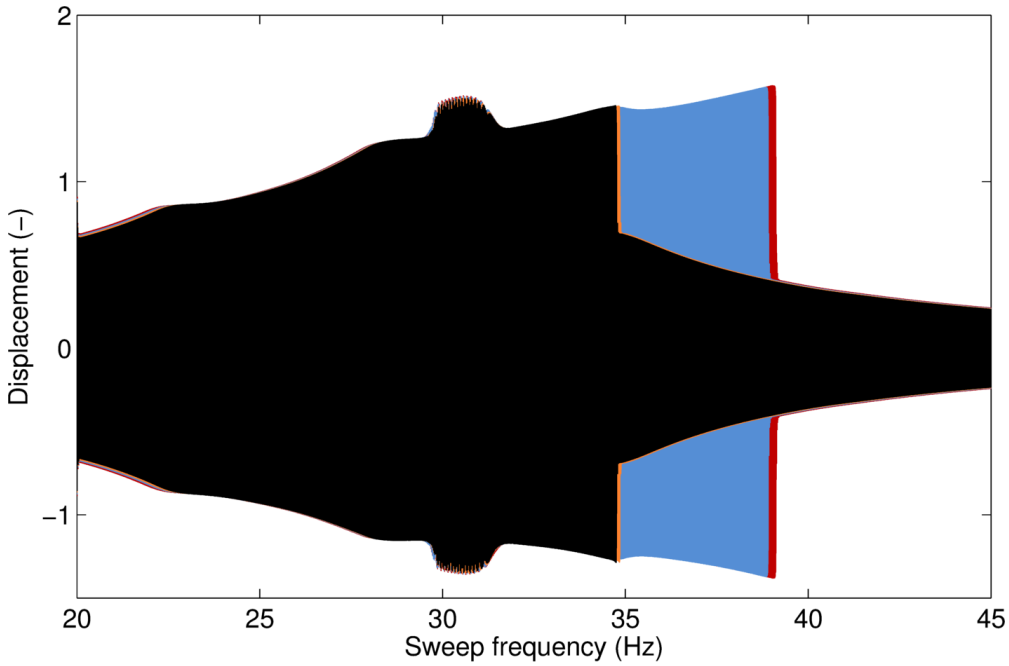

(b)

Fig. 6. Time series computed from the numerical model. (a) Swept-sine response in acceleration of the instrument panel at P-Z for a forcing amplitude of $f = 20$ N (in orange) and $f = 80$ N (in black); (b) swept-sine response in displacement of the inertia wheel at NC1-Z for a forcing amplitude $f = 168$ N (in black), $f = 170$ N (in orange), $f = 172$ N (in blue) and $f = 174$ N (in red).

If these simulations confirm the good predictive capabilities of the model and highlight new phenomena, an explanation of the underlying dynamical mechanisms is yet to be provided. This is the objective of Sections 4 and 5, which apply the NNM theory and bifurcation analysis to the spacecraft, respectively.

5. UNDERSTANDING NONLINEAR RESONANCES THROUGH MODAL ANALYSIS

Because of the presence of the nonlinearities, the model of the SmallSat has a feature typical of nonlinear systems: its oscillations are frequency-energy dependent. In order to assess this dependence, the framework of Nonlinear Normal Modes (NNMs) proposed by Vakakis et al. [10], and Kerschen et al. [11], is employed. The concept of NNM can be seen as a nonlinear generalization of the concept of Linear Normal Mode (LNM) of classical linear vibration theory: a NNM is a (nonnecessarily synchronous) periodic motion of the underlying conservative system. In order to describe a NNM, one thus has to provide an initial state for the system (displacements and velocities) whose free response leads to periodic oscillation of the DOFs with a dominant frequency ω. Since the system is conservative, the total (kinetic and potential) energy level E related to its state does not evolve during the simulation.

A convenient tool to depict the NNMs, the Frequency-Energy Plot (FEP), consists in representing the evolution of the frequency ω with respect to the energy level E. This procedure facilitates the identification of families of NNMs sharing the same qualitative properties (a global in-phase motion for example). The FEP depicted in Fig. 7 shows the sixth family of NNMs of the underlying undamped model of the SmallSat, computed with the shooting technique [12]. At low energy levels, the metallic cross does not interact with the mechanical stops. Consequently, the frequency of the NNMs does not depend on energy, and remains the same as the frequency of the linear mode. For larger energy levels, nonlinearities are activated. The frequency of the NNMs increases suddenly and rapidly, resulting from the nonsmooth and hardening nature of the nonlinearities.

A closer look on frequencies above 28.8 Hz in Fig. 7 highlights another feature of nonlinear systems: the internal resonances (IRs), or modal interactions, between the nonlinear modes. Because the sixth NNM branch does not have the same dependence in energy as the other NNM branches, in some regions these branches can have commensurate frequencies. For example, in the case of a 2:1 resonance, at a given energy a solution along the branch of NNM 6 has a frequency which is exactly 2 times smaller than the frequency of another solution along the branch of NNM 12. Because a solution 2ω-periodic is also ω-periodic, the two modes interact and the periodic solutions resulting from this interaction appears as a small part, termed tongue, emanating from the main branch, called backbone, in the FEP. When progressing along the IR, a dynamic coupling between the two modes is established together with an energy transfer. Four different internal resonances are depicted in Fig. 7, namely 2:1, 26:1, 3:1 and 9:1.

The mode shapes related to NNMs computed in the linear regime and at the extremity of the 2:1 IR are also depicted in Fig. 7. The sixth linear mode shape mainly involves vertical motion of the inertia wheel. Very interestingly, on the 2:1 IR tongue, the mode shape becomes a mixing between the shapes of NNM6 and NNM12 until, at the extremity, the sole second harmonic remains, which completes a transition to NNM12. This latter NNM is associated with strong instrument panel motion. The nonlinear resonance observed in Fig. 3 and Fig. 6(a) can therefore be attributed to a 2:1 modal interaction between the sixth and the twelfth modes of the spacecraft.

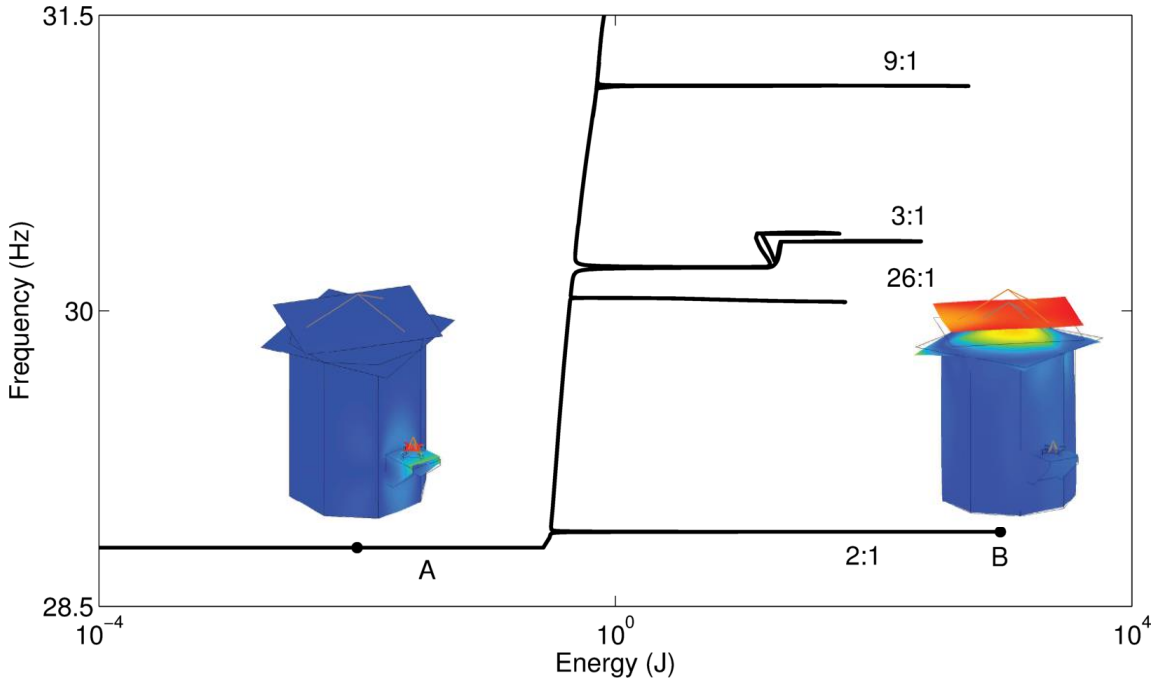

Fig. 7. Representation of the sixth NNM on the FEP and of the mode shapes at A and B.

6. UNCOVERING NONLINEAR PHENOMENA THROUGH BIFURCATION ANALYSIS

The present section is dedicated to the study of the response of the satellite to harmonic excitation applied to the vertical DOF of the inertia wheel. More specifically, an explanation of the nonlinear phenomena observed in Fig. 6(b) is sought. The nonlinear frequency response curves (NFRCs) and bifurcation curves presented in this section are computed using a continuation procedure based on the harmonic balance formalism described in [5], with 5 harmonics retained.

Detection of bifurcations

Fig. 8 depicts the system's NFRCs at NC1-Z for forcing amplitudes of $f = 155$ N. Circle and triangle markers denote the fold and Neimark-Sacker (NS) bifurcations, respectively, that are detected along the branch. A pair of fold bifurcations is found in the bending segments of the resonance peak, which is due to the hardening behavior of the system. A pair of NS bifurcations can also be observed, which means that quasiperiodic (QP) solutions may emanate in their vicinity. As a verification, the response to a swept-sine excitation with a forcing amplitude of 155 N computed with a Newmark time integration scheme is also superposed to the NFRC. Along with the fact that the NFRC provide accurate estimations of the displacement envelopes, as expected, one notes that the bifurcations are directly related to the nonlinear phenomena observed in Fig. 6(b). On the one hand, fold bifurcations accurately point out the location of the amplitude jump; indeed, fold bifurcations give rise to a change in stability of the periodic solutions. On the other hand, the modulation of the displacement's envelope near 30 Hz can be explained by the creation of a branch of stable QP oscillations at the NS bifurcations.

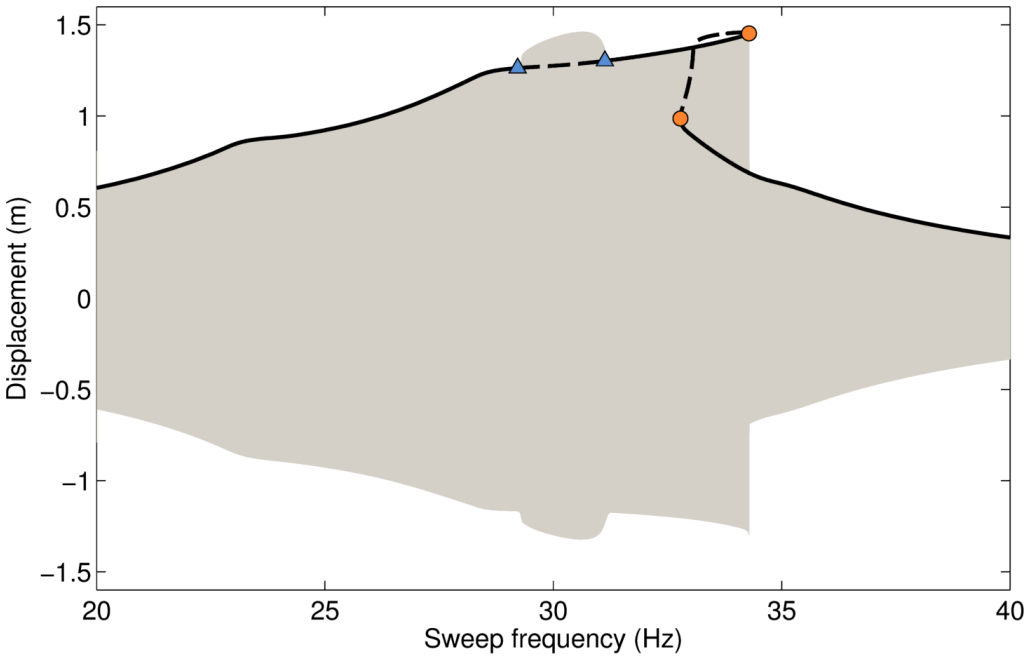

Fig. 8. NFRC and stability analysis for $f = 155$ N. Comparison between the NFRC (in black) and the swept-sine response calculated at NC1-Z using time integration (in grey). Circle and triangle markers represent fold and NS bifurcations, respectively. The solid and dashed lines represent stable and unstable branches, respectively.

Investigation of the frequency shift

As fold bifurcations are located close to resonance peaks, tracking their evolution with respect to other parameters such as the forcing amplitude f or the axial damping c_{ax} in the elastomer plots could reveal the mechanism of the frequency shift shown in Fig. 6(b). To this end, a tracking of the fold bifurcations in the codimension-2 forcing frequency-ω and amplitude-f space is performed using the technique developed in [5]. Fig. 9(a) represents the fold curve obtained, together with the NFRCs of the system for different forcing levels. Fig. 9(b) also shows the projection of this curve in the f-amplitude plane. Very interestingly, the fold branch first tracks the bifurcations of the main frequency response, and then turns back to reveal isolated response curves (IRCs), or isolas, which are rarely observed for such large systems. These IRCs are created around the resonance peak at a forcing amplitude $f = 158$ N, then expands both in frequency and amplitude, until one reaches a forcing amplitude $f = 170$ N at which they merge with this resonance peak. It can be shown that the upper part of the IRC is stable; as a direct consequence, the merging of the IRC with the resonance peak leads to the sudden increase of the latter in frequency and amplitude, as highlighted in Fig. 6(b).

Another fold curve is computed for a configuration of the SmallSat with an axial damping $c_{ax} = 85$ Ns/m slightly higher than its reference value $c_{ax} = 63$ Ns/m, and represented in dashed line in Fig. 9(b). While an increase in damping could be expected to annihilate nonlinear phenomena such as IRCs, it only postpones the merging to higher forcing amplitudes and does not alter the size of the IRCs. For this system, IRCs are thus robust and deserve a careful investigation from the structural engineers.

Together with the explanations about the SmallSat dynamics they provide, these first results show that crucial information can be missed when one only performs continuation of periodic solutions. Obviously, a tracking in codimension-2 space is necessary in order to reveal IRCs.

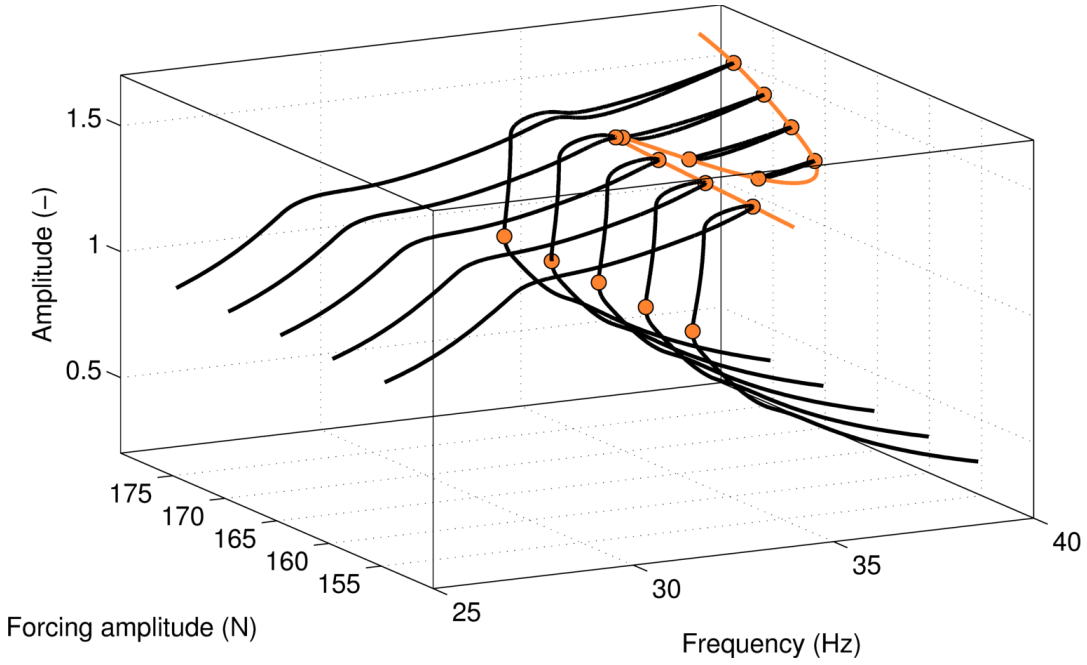

(a)

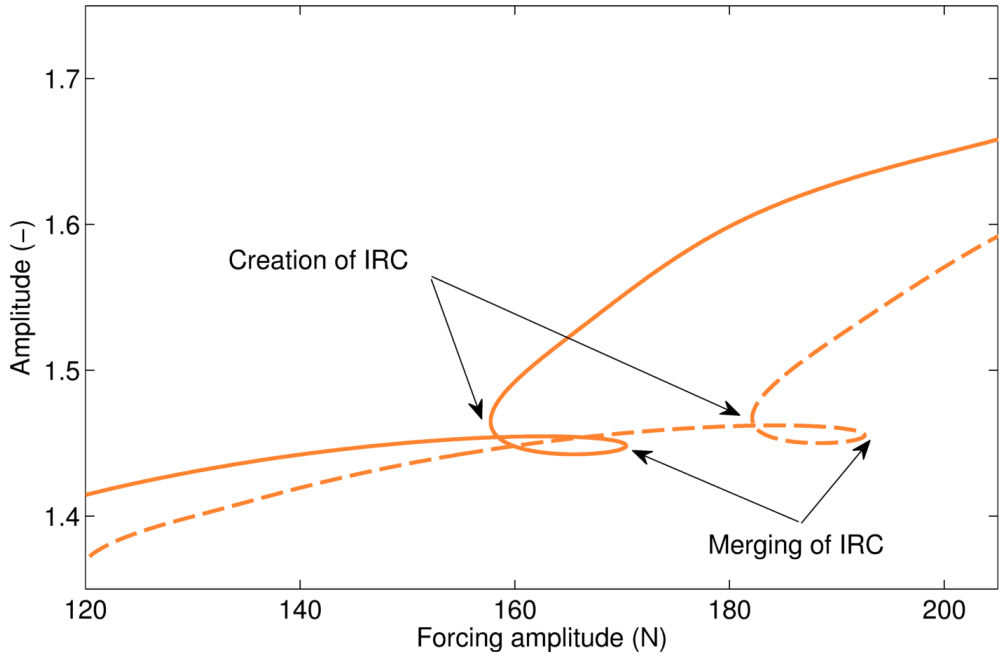

(b)

Fig. 9. Tracking of the fold bifurcations of the resonance peak. (a) Three-dimensional space. Branch of fold bifurcations (in orange), NFRCs computed at NC1-Z for $f = 155$ N, 160 N, 170 N and 175 N (in black). Circle markers depict fold bifurcations; (b) two-dimensional projection of the branch of fold bifurcations for $c_{ax} = 63$ Ns/m (reference, solid line) and $c_{ax} = 85$ Ns/m (dashed line).

7. NONLINEAR DESIGN THROUGH BIFURCATION ANALYSIS

The QP oscillations observed in Fig. 6(b) are created and eliminated at the first and second NS bifurcations, respectively; tracking the evolution of NS bifurcations with respect to a design parameter such as the axial damping c_{ax} could then indicate how the design of the SmallSat can be modified to avoid such disturbances.

Fig. 10(a) depicts the evolution of the NS curve in the codimension-2 forcing frequency-ω and axial damping-c_{ax} space, to which one superimposes NFRCs computed for $c_{ax} = 63$ Ns/m, 80 Ns/m and 85 Ns/m. Its projection in the c_{ax}-amplitude plane is also given in Fig. 10(b). It is interesting to note that increasing the axial damping up to a value of 84 Ns/m eliminates the NS bifurcations, while it does not significantly affect the resonance peaks.

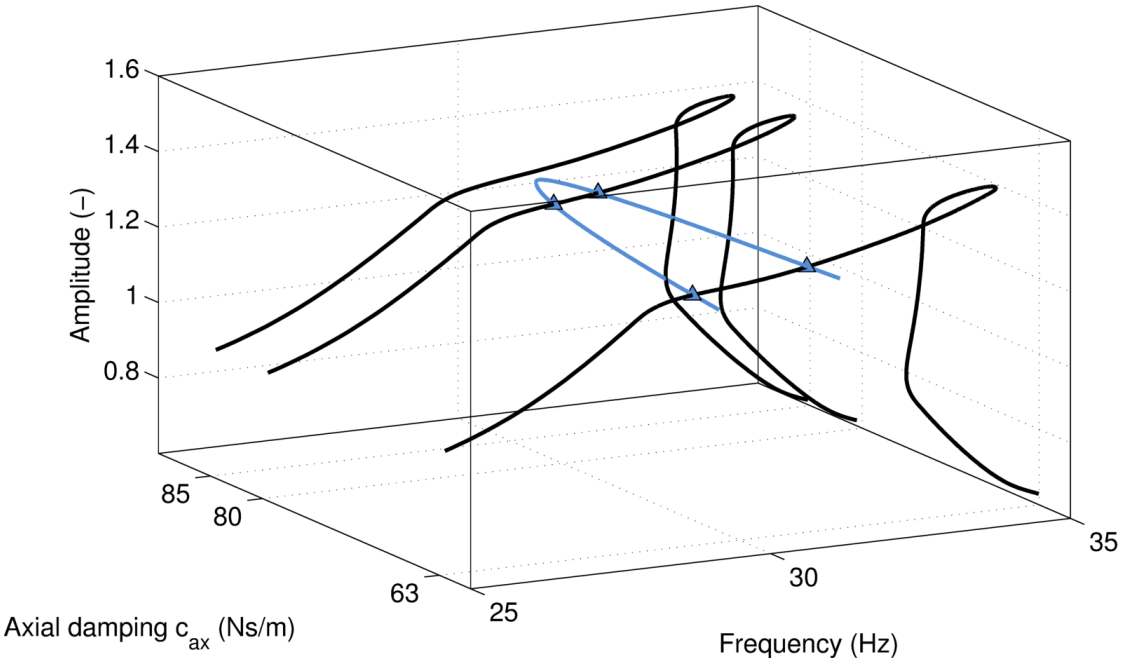

(a)

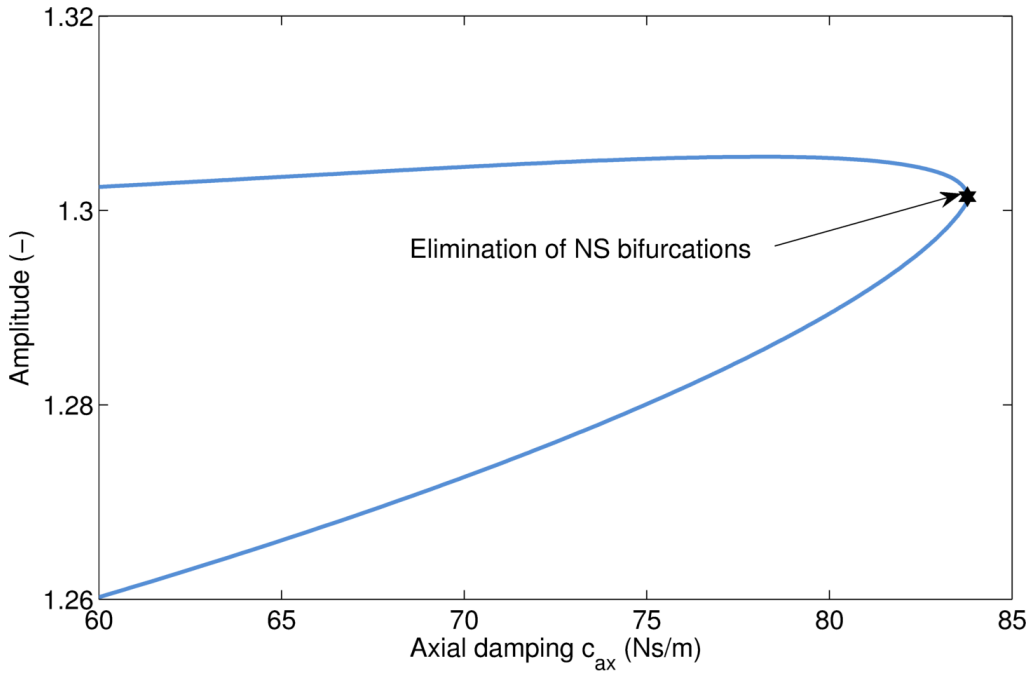

(b)

Fig. 10. Tracking of the NS bifurcations. (a) Three-dimensional space. Branch of NS bifurcations (in blue), NFRCs computed at NC1-Z for $f = 155$ N and for $c_{ax} = 63$ Ns/m, 80 Ns/m and 85 Ns/m (in black). Triangle markers depict NS bifurcations; (b) two-dimensional projection of the branch of NS bifurcations.

As a verification, Fig. 11 shows the influence of c_{ax} on a displacement response for swept-sine excitations. At a forcing amplitude $f = 155$ N and for an axial damping $c_{ax} = 63$ Ns/m, the QP oscillations represent the part of the response with the largest amplitude. Increasing c_{ax} up to 85 Ns/m eliminates the NS bifurcations which generate these disturbances, with a small impact on the frequency of the resonance.

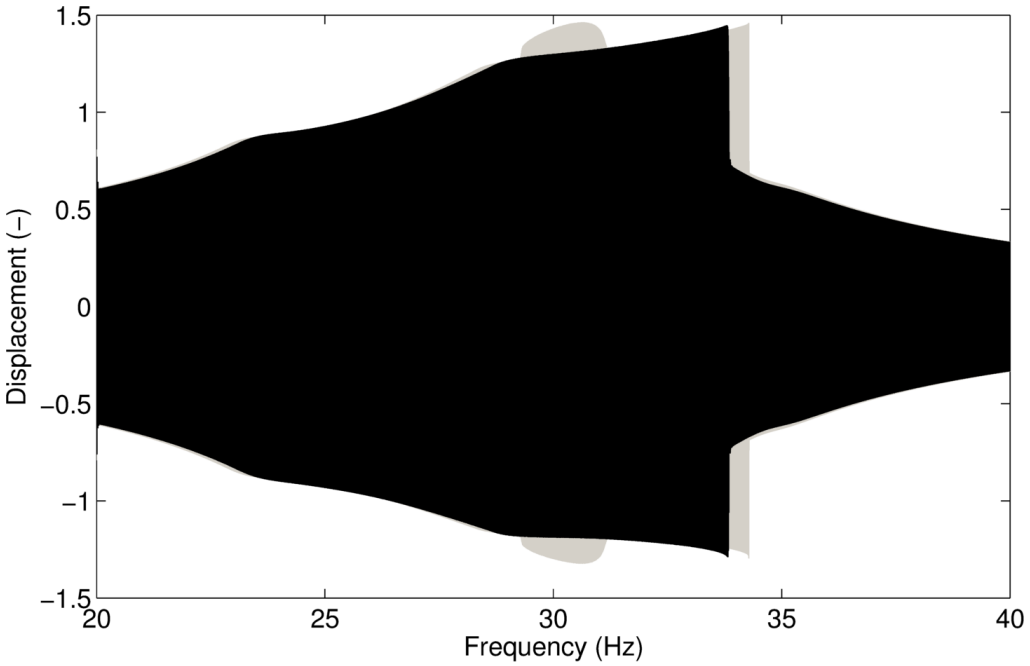

Fig. 11. Influence of the damping value c_{ax} on the response at NC1-Z to swept-sine excitation, computed for $f = 155$ N and for $c_{ax} = 63$ Ns/m (reference, in grey) and $c_{ax} = 85$ Ns/m (in black).

8. CONCLUSIONS

In this paper, nonlinear experimental and numerical techniques were applied to the SmallSat spacecraft, an industrial and complex model with several localized nonlinearities. Performing swept-sine excitation studies on this structure revealed three types of nonlinear phenomena, namely modal interactions, quasiperiodic oscillations and frequency/amplitude jumps. A nonlinear numerical model of the spacecraft was then exploited not only to understand the measured nonlinear regimes of motion, but also to uncover what additional nonlinear phenomena, such as isolated response curves, can be encountered in the different regimes of operation of the structure.

Eventually, this process allows the structural analyst to precisely quantify the impact of nonlinearity and to decide whether design modifications are necessary to achieve the requested system performance.

ACKNOWLEDGMENTS

The authors T. Detroux, L. Masset and G. Kerschen would like to acknowledge the financial support of the European Union (ERC Starting Grant NoVib 307265). The author J.P. Noël is a Postdoctoral Researcher of the Fonds de la Recherche Scientifique - FNRS which is also gratefully acknowledged.

REFERENCES

[1] S.F. Masri and T.K. Caughey, *A nonparametric identification technique for nonlinear dynamic problems*, Journal of Applied Mechanics, 46(2):433–447, 1979.

[2] P. Muhamad, N.D. Sims and K. Worden, *On the orthogonalised reverse path method for nonlinear system identification*, Journal of Sound and Vibration, 331(20):4488–4503, 2012.

[3] J.P. Noël and G. Kerschen, *Frequency-domain subspace identification for nonlinear mechanical systems*, Mechanical Systems and Signal Processing, 40(2):701–717, 2013.

[4] M. Géradin and D.J. Rixen, *Mechanical Vibrations: Theory and Application to Structural Dynamics*, John Wiley & Sons, New-York, NY, 2014.

[5] T. Detroux, L. Renson, L. Masset and G. Kerschen, *The harmonic balance method for bifurcation analysis of large-scale nonlinear mechanical systems*, Computer Methods in Applied Mechanics and Engineering, 296:18–38, 2015.

[6] A.G. Russell, *Thick skin, faceted, CFRP, monocoque tube structure for smallsats*, In Proceedings of European Conference on Spacecraft Structures, Materials and Mechanical Testing, Noordwijk, The Netherlands, 2000.

[7] J.P. Noël, L. Renson and G. Kerschen, *Complex dynamics of a nonlinear aerospace structure: Experimental identification and modal interactions*, Journal of Sound and Vibration, 333(12):2588–2607, 2014.

[8] M.C.C. Bampton and J.R.R. Craig, *Coupling of substructures for dynamic analyses*, AIAA Journal, 6(7):1313–1319, 1968.

[9] L. Renson, J.P. Noël and G. Kerschen, *Complex dynamics of a nonlinear aerospace structure: Numerical continuation and normal modes*, Nonlinear Dy-namics, 79(2):1293–1309, 2015.

[10] A.F. Vakakis, L.I. Manevitch, Y.V. Mikhlin, V.N. Pilipchuk and A.A. Zevin, *Normal modes and localization in nonlinear systems*, John Wiley & Sons, New-York, NY, 2008.

[11] G. Kerschen, M. Peeters, J.-C. Golinval and A.F. Vakakis, *Nonlinear normal modes, Part I: A useful framework for the structural dynamicist*, Mechanical Systems and Signal Processing, 23(1):170–194, 2009.

[12] M. Peeters, R. Viguié, G. Sérandour, G. Kerschen and J.C. Golinval, *Nonlinear normal modes, Part II: Toward a practical computation using numerical continuation techniques*, Mechanical Systems and Signal Processing, 23(1):195–216, 2009.